

Collective excitations of dynamic Fermi surface deformations in $\text{BaFe}_2(\text{As}_{0.5}\text{P}_{0.5})_2$

S.-F. Wu,^{1,2} W.-L. Zhang,² D. Hu,² H.-H. Kung,¹ A. Lee,¹ H.-C. Mao,²
P.-C. Dai,³ H. Ding,^{2,4,*} P. Richard,^{2,4,*} and G. Blumberg^{1,5,†}

¹*Department of Physics and Astronomy, Rutgers University, Piscataway, NJ 08854, USA*

²*Beijing National Laboratory for Condensed Matter Physics,*

and Institute of Physics, Chinese Academy of Sciences, Beijing 100190, China

³*Department of Physics and Astronomy, Rice University, Houston, Texas 77005, USA*

⁴*Collaborative Innovation Center of Quantum Matter, Beijing, China*

⁵*National Institute of Chemical Physics and Biophysics, 12618 Tallinn, Estonia*

(Dated: March 5, 2024)

We use electronic Raman scattering to study the low-energy excitations in $\text{BaFe}_2(\text{As}_{0.5}\text{P}_{0.5})_2$ ($T_c \approx 16$ K) samples. In addition to a superconducting pair breaking peak ($2\Delta = 6.7$ meV) in the A_{1g} channel with a linear tail towards zero energy, suggesting a nodal gap structure, we detect spectral features associated to Pomeranchuk oscillations in the A_{1g} , B_{1g} and B_{2g} channels. We argue that the small Fermi energy of the system is an essential condition for these Pomeranchuk oscillations to be underdamped. The Pomeranchuk oscillations have the same frequencies in the B_{1g} and B_{2g} channels, which we explain by the mixing of these symmetries resulting from the removal of the σ_v and σ_v symmetry planes due to a large As/P disorder. Interestingly, we show that the temperature at which the peaks corresponding to the Pomeranchuk oscillations get underdamped is consistent with the non-Fermi liquid to Fermi liquid crossover determined by transport, suggesting that the Pomeranchuk instability plays an important role in the low-energy physics of the Fe-based superconductors.

PACS numbers: 74.70.Xa, 74.74.25.nd

With their multiband nature, the Fe-based superconductors provide an interesting playground for studying many-body effects and collective excitations. Of particular interest is the role played by the degeneracy of the d_{xz} and d_{yz} orbitals. Many Fe-based superconductors exhibit an antiferromagnetic phase transition that is preceded by a small structural distortion at a temperature T_s that removes the degeneracy between the d_{xz} and d_{yz} orbitals. For $\text{BaFe}_2(\text{As}_{1-x}\text{P}_x)_2$, evidence was shown for the existence of quantum critical behavior at $x = 0.3$ [1–4], which coincides with the composition at which T_s drops to zero. At that particular doping, the electrical resistivity $\rho(T)$ at high temperature varies linearly [2, 4], which is attributed to a non-Fermi liquid (NFL) behavior. This NFL behavior is found over a wide range of temperature and P concentration, and it is separated by a crossover from a Fermi liquid (FL) like regime with $\rho(T) \sim T^2$ [4].

Mainly due to the complexity of the interplay between the spin and orbital degrees of freedom [5], there is still no consensus on the precise nature of the critical fluctuations preceding the magnetic and structural transitions, which may also be responsible for the observed NFL behavior. Recently, Raman scattering studies evidenced the existence of quadrupolar charge fluctuations with the B_{2g} symmetry above T_s in $\text{NaFe}_{1-x}\text{Co}_x\text{As}$ [6], $\text{Ba}(\text{Fe}_{1-x}\text{Co}_x)_2\text{As}_2$ [7, 8], AFe_2As_2 [$A = (\text{Sr}, \text{Eu})$] [9] and FeSe [10]. Such Pomeranchuk like instability [11], where the Fermi surface (FS) encounters dynamical deformation,

is a natural consequence of the degeneracy of the d_{xz} and d_{yz} orbitals at high temperature. The corresponding susceptibility, which can be probed directly by Raman scattering, diverges as approaching the Pomeranchuk instability. However, there is to date no experimental correlation between the Pomeranchuk fluctuations [11, 12] and the NFL behavior observed in $\text{BaFe}_2(\text{As}_{1-x}\text{P}_x)_2$, and whether the fluctuations may appear in the other symmetry channels, is unclear.

In this Letter, we use electronic Raman scattering to study the low-energy excitations in $\text{BaFe}_2(\text{As}_{0.5}\text{P}_{0.5})_2$ ($T_c \approx 16$ K), for which there is neither long-range magnetic nor long-range nematic ordering. We reveal evidence for Pomeranchuk oscillations in different symmetry channels, with frequencies larger than the superconducting (SC) gap determined from a SC pair breaking peak ($2\Delta = 6.7$ meV) in the A_{1g} channel. We argue that the small Fermi energy of the system is an essential condition for these Pomeranchuk oscillations to be underdamped. No sharp collective mode is observed below the SC gap, possibly due to the nodal nature of the SC gap structure derived from the finite and linear Raman response towards zero energy in the A_{1g} channel. Interestingly, the Pomeranchuk oscillations have the same frequency in the B_{1g} and B_{2g} channels, which we explain by the mixing of these symmetries resulting from the removal of the σ_v and σ_v symmetry planes due to a large As/P disorder. More importantly, we show that the temperature at which the peaks corresponding to the Pomeranchuk oscillations get underdamped is consistent with the FL to NFL crossover determined by transport. This suggests that the Pomeranchuk instability plays an essential role

* p.richard@iphy.ac.cn

† girsh@physics.rutgers.edu

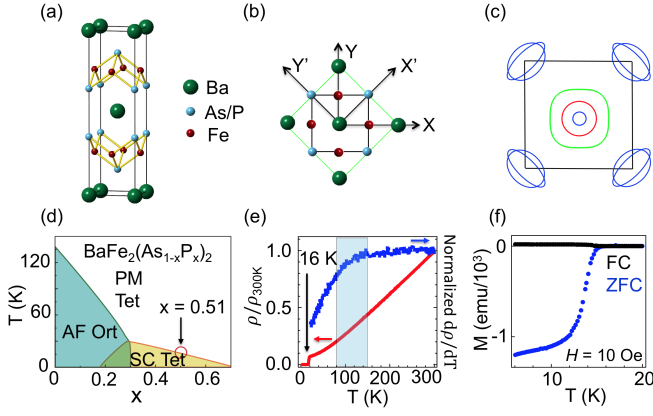


FIG. 1. (Color online) Properties of $\text{BaFe}_2(\text{As}_{0.5}\text{P}_{0.5})_2$. (a) Crystal structure of $\text{BaFe}_2(\text{As}_{0.5}\text{P}_{0.5})_2$. (b) Definition of the X, Y, X' and Y' directions. The green and black lines represent the 4-Fe and 2-Fe unit cells, respectively. (c) Schematic representation of the FSs in the 2-Fe Brillouin zone in the $k_z = \pi$ plane [14, 15]. (d) Schematic phase diagram of $\text{BaFe}_2(\text{As}_{1-x}\text{P}_x)_2$ [16]. (e) Normalized resistivity (red) and its normalized derivative (blue). The shadow area indicates a crossover from quadratic to linear temperature dependence. (f) Magnetic susceptibility in field-cooled (FC) and zero-field-cooled (ZFC) modes.

in shaping the electronic properties of Fe-based superconductors.

Single crystals of $\text{BaFe}_2(\text{As}_{0.5}\text{P}_{0.5})_2$ were grown using the $\text{Ba}_2\text{As}_3/\text{Ba}_2\text{P}_3$ self-flux method described in Ref. [13], and the chemical compositions were determined by inductive coupled plasma analysis. The crystal structure, illustrated in Figs. 1(a) and 1(b), belongs to space group $I4/mmm$ (point group D_{4h}). Resistivity (Fig. 1(e)) and magnetic susceptibility (Fig. 1(f)) measurements indicate $T_c \approx 16$ K. The crystals used for Raman scattering were cleaved and positioned in a continuous He flow optical cryostat. The measurements presented here were performed in a quasi-back scattering geometry along the crystallographic c -axis using the Kr^+ laser line at 647.1 nm (1.92 eV). The excitation laser beam was focused into a $50 \times 100 \mu\text{m}^2$ spot on the ab -surface, with the incident power smaller than 10 and 6 mW for measurements in the normal state and in the SC state, respectively. The scattered light was collected and analyzed by a triple-stage Raman spectrometer designed for high-stray light rejection and throughput, and then recorded using a liquid nitrogen-cooled charge-coupled detector. Raman spectra were recorded in the range of 10 to 350 cm^{-1} using a 1800 grooves/mm grating and in the range of 100 to 2000 cm^{-1} using a 150 grooves/mm grating. Raman scattering intensity data were corrected for the spectral responses of the spectrometer and detector. The temperature has been corrected for laser heating.

In this manuscript, we define X and Y along the 2-Fe unit cell basis vector (at 45° degrees from the Fe-Fe direction) in the tetragonal phase, whereas X' and Y' are

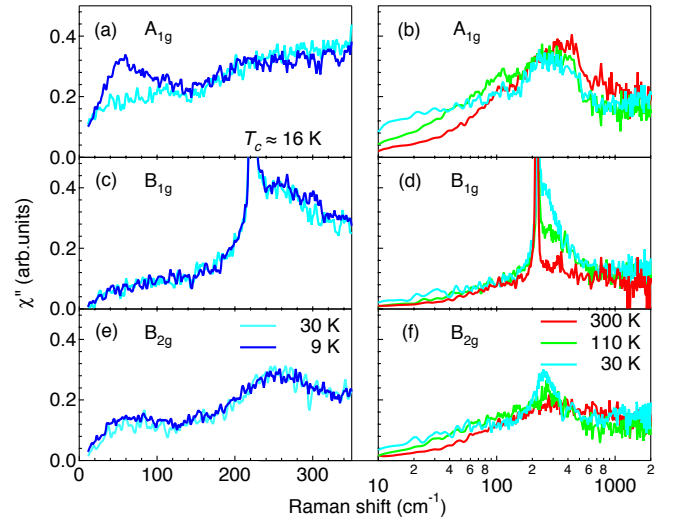


FIG. 2. (Color online) Raman response $\chi''_{A_{1g}}(\omega, T)$ in (a-b), $\chi''_{B_{1g}}(\omega, T)$ in (b-c) and $\chi''_{B_{2g}}(\omega, T)$ in (c-d) of $\text{BaFe}_2(\text{As}_{0.5}\text{P}_{0.5})_2$ at different temperatures.

along the Fe-Fe directions, as shown in Fig. 1(b). We also define R and L as circular right and circular left polarizations. The static Raman susceptibility $\chi'(0, T)$ was obtained from a Kramers-Kronig transformation with a high-energy cut-off at 350 cm^{-1} . The B_{1g} phonon was removed by fitting before the Kramers-Kronig transformation in the B_{1g} channel.

The Raman selection rules for crystals with the D_{4h} point group symmetry indicate that the XX, XY, X'X', X'Y', RR, RL polarization geometries probe the $A_{1g} + B_{1g}$, $A_{2g} + B_{2g}$, $A_{1g} + B_{2g}$, $A_{2g} + B_{1g}$, $A_{1g} + A_{2g}$ and $B_{1g} + B_{2g}$ channels, respectively. Assuming a same featureless luminescence background I_{BG} for all symmetry channels and that the A_{2g} response is negligible, the imaginary part of the Raman susceptibility χ'' in the different symmetry channels can easily be isolated.

In Figs. 2(a)-2(b), we show the Raman susceptibility $\chi''_{A_{1g}}(\omega, T)$ at different temperatures from 300 K to 9 K. The most prominent feature that appears in the low-energy part of the A_{1g} channel (Fig. 2(a)) is a peak emerging at 54 cm^{-1} (6.7 meV) at 9 K, in the SC state. Tentatively ascribing this feature to a pair breaking peak would lead to $2\Delta = 6.7 \text{ meV}$. Such value is about twice lower than the values of SC gaps reported by ARPES for the optimal- T_c compound [17], for which T_c is about twice larger. Another possible interpretation for this peak, also related to superconductivity, is an electron-hole plasmonic excitation inside the SC gap, as reported earlier in $\text{NaFe}_{1-x}\text{Co}_x\text{As}$ [6]. Unlike the expectation for a completely open gap, the spectral intensity decreases linearly towards the low frequencies, indicating the presence of excitations with energy lower than 2Δ . This suggests that the SC gap probed in the A_{1g} channel is nodal. Although the detail of the SC gap structure measured by

ARPES on $\text{BaFe}_2(\text{As}_{1-x}\text{P}_x)_2$ is still controversial [17–19], strong SC gap anisotropy [19] and even an horizontal line node [17] have been proposed. A nodal gap structure is also inferred from thermal conductivity measurements [20, 21].

In Fig. 2(b), we show the A_{1g} Raman spectra up to 2000 cm^{-1} in a semi-log plot. We detect a broad peak centered around 350 cm^{-1} , with a full-width-at-half-maximum (FWHM) of about 300 cm^{-1} . Upon cooling, this peak shows some temperature dependence, but the most obvious changes occur in the low-energy part of the spectrum, which is enhanced at low temperature.

The $\chi''_{B_{1g}}(\omega, T)$ susceptibility displayed in Figs. 2(c)–2(d) shows a sharp peak at 218 cm^{-1} (300 K) that is ascribed to a B_{1g} phonon [22]. It corresponds to the vibration of Fe atoms along the c axis. A peak at 260 cm^{-1} develops upon cooling on the right side of the phonon mode. This peak is asymmetric, with a high-energy tail extending to 800 cm^{-1} , as shown in Fig. 2(d). The peak reaches half of its highest intensity at 110 K, and its maximum intensity saturates at low temperature, with no obvious change across T_c (see Fig. 2(c)). The temperature dependence of the FWHM, displayed in Fig. 3(a), is nearly 200 cm^{-1} at 9 K, which leads to a quality factor (QF) of 1.3 (underdamped regime). In contrast, QF smaller than 0.5 (overdamped regime) is observed for a FWHM larger than 520 cm^{-1} , which occurs slightly above 100 K.

A recent study of the resistivity across the phase diagram of $\text{BaFe}_2(\text{As}_{1-x}\text{P}_x)_2$ revealed a crossover between a regime with $\rho(T) \sim T$ at high temperature and a regime $\rho(T) \sim T^2$ at low temperature [4]. As shown by the first derivative of the resistivity in Fig. 1(e), this is also what we find in our samples, with a crossover regime spanning from about 80 to 150 K. As indicated by the shadow area in Fig. 3(a), this temperature regime coincides with the temperature at which the Raman peak at 260 cm^{-1} switches from overdamped to underdamped ($\text{QF} = 1/2$), suggesting that Raman scattering probes the same crossover as measured in transport.

Interestingly, the $\chi''_{B_{2g}}(\omega, T)$ susceptibility displayed in Figs. 2(e)–2(f) also shows a peak at 260 cm^{-1} that is absent at 300 K but gets enhanced upon cooling. The broadness of the peak and the temperature at which it appears are very similar to what is observed for the 260 cm^{-1} mode detected in the B_{1g} channel, suggesting that these two peaks have the same origin. Although such degeneracy is not expected within the D_{4h} point group symmetry, one can argue that the randomness of the As-P distribution near $x = 0.5$ locally breaks the σ_v and σ_d symmetry planes, allowing mixing the B_{1g} and B_{2g} symmetries. In fact, the absence in our data of the A_{1g} pnictogen phonon mode observed in other Fe-based superconductors [6, 22–24], is a good indication of the disorder effect. We caution that since As and P are isovalent, the removal of the σ_v and σ_d symmetry planes is a relatively weak perturbation that would not affect modes that do not involve the pnictogen atoms, such as the Fe-related B_{1g} phonon, which remains sharp and for

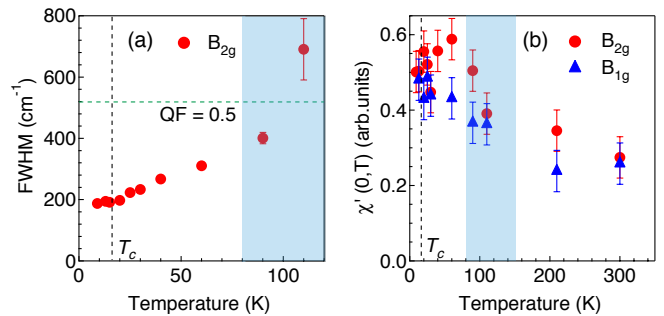


FIG. 3. (Color online) (a) Static Raman susceptibility $\chi'(0, T)$ in the B_{1g} (blue triangles) and B_{2g} (red circles) channels. The green horizontal dashed line corresponds to critical damping ($\text{QF} = 1/2$). (b) FWHM of the 260 cm^{-1} peak in the B_{2g} channel. The vertical dashed lines and the blue shadow areas in (a) and (b) indicate T_c and the crossover from T^2 to T resistivity, respectively.

which no leak is detected in the B_{2g} channel. In addition to the peak at 260 cm^{-1} , we observe in the B_{2g} channel an extra peak at 60 cm^{-1} that shows enhancement in the SC state.

We show the temperature dependence of $\chi'(0, T)$ in Fig. 3(b). The $\chi'(0, T)$ obtained in both channels is enhanced gradually upon cooling from 300 K to around 50 K, *i. e.* above T_c , before being gradually weakened at lower temperature. The increase of $\chi'(0, T)$ is possibly due to the low-frequency relaxation across the NFL to FL crossover indicated by a shadow area in Fig. 3(b).

We now try to provide a physical picture for the mode at 260 cm^{-1} . In recent Raman scattering studies the presence of a low-energy excitation with the B_{2g} symmetry is interpreted in terms of quadrupolar charge fluctuations [orbital singlet excitations ($\Delta L = 2$) or Pomeranchuk instability [6, 8–10]. Indeed, a dynamic charge quadrupole moment of B_{2g} symmetry (nodes along the X-Y directions) can form locally on Fe sites due to the fluctuating partial charge transfer between degenerate d_{xz} and d_{yz} orbitals in the tetragonal phase [6, 9]. In Fig. 4(b), we show a cartoon of B_{2g} symmetry charge transfer oscillation from d_{xz} to d_{yz} . In momentum space, the charge transfer leads to dynamical FS distortions of the d_{xz}/d_{yz} bands with nodes along Γ -X and Γ -Y, as illustrated in Fig. 4(g). In $\text{NaFe}_{1-x}\text{Co}_x\text{As}$, the peak corresponding to the quadrupolar charge fluctuations is found at low energy [6]. Above T_c , the excitation is broad and it gets completely overdamped at high temperature. However, below T_c the mode becomes extremely sharp due to the absence of low-energy particle-hole excitations following a full SC gap opening [25–27].

Because the FS topology of $\text{BaFe}_2(\text{As}_{0.5}\text{P}_{0.5})_2$ is similar to that of $\text{NaFe}_{1-x}\text{Co}_x\text{As}$, one should also expect to observe Pomeranchuk oscillations in $\text{BaFe}_2(\text{As}_{0.5}\text{P}_{0.5})_2$, with the B_{2g} symmetry. For this reason, it is natural to attribute the origin of the mode at 260 cm^{-1} to charge quadrupole fluctuations. However, we caution that the

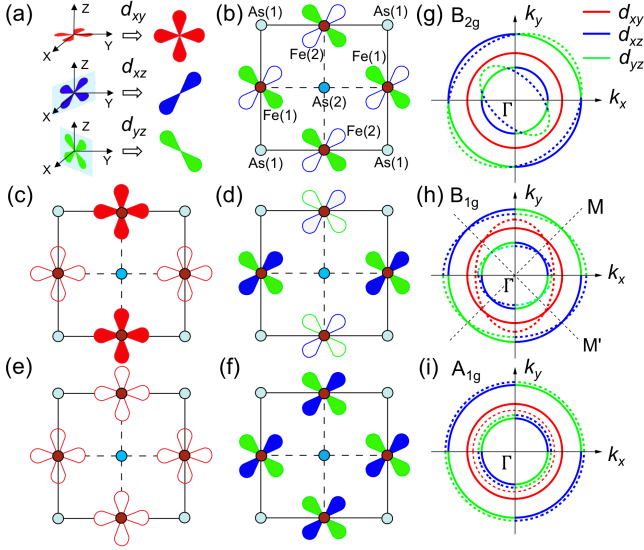


FIG. 4. (Color online) Cartoons of symmetrized Pomeranchuk oscillations in real and momentum spaces. (a) Real space orientation of the d_{xy} and d_{xz}/d_{yz} orbitals. (b) B_{2g} type charge transfer within the d_{xz}/d_{yz} orbitals. Adjacent Fe sites are labeled Fe(1) and Fe(2). As sites above and below the Fe plane are labeled As(1) and As(2). (c-d) shows B_{1g} type anti-phase charge transfer from d_{xy} to d_{xz}/d_{yz} orbitals on one Fe site and the opposite direction on a neighbor site. (e-f) A_{1g} type of in-phase charge transfer from d_{xy} to d_{xz}/d_{yz} orbitals on all Fe sites. FS deformations of (g) B_{2g} type, (h) B_{1g} type, and (i) A_{1g} type.

physical situation may be different in $\text{BaFe}_2(\text{As}_{0.5}\text{P}_{0.5})_2$. For example, the SC gap in $\text{BaFe}_2(\text{As}_{0.5}\text{P}_{0.5})_2$ may be nodal, as discussed above, and thus particle-hole excitations can always damp the Pomeranchuk oscillations, thus preventing the emergence of a very sharp mode at low energy, in the SC phase. With a QF of 1.3, the mode at 260 cm^{-1} , above the SC gap, is quite sharp. This underdamped mode is possible only if the Pomeranchuk oscillation frequency ω_B is large compared to thermal fluctuations and to the Fermi energy of the system. The first condition, $T \ll \omega_B$, is respected since 260 cm^{-1} corresponds to a thermal energy of 374 K. Based on ARPES data on $\text{BaFe}_2(\text{As}_{0.5}\text{P}_{0.5})_2$ [28], we estimate that while the holelike d_{xy} band tops at about 30 meV at the Γ point, the two d_{xz}/d_{yz} bands top at 10 meV and 15 meV. This means that the Fermi energy of the system is smaller than ω_B , which is consistent with underdamped Pomeranchuk oscillations ($\text{QF} > 1/2$).

As discussed previously, it is likely that the 260 cm^{-1} excitation in the B_{1g} channel is related to the Pomeranchuk oscillation found in the B_{2g} channel at the same energy. We note that $\text{BaFe}_2(\text{As}_{0.5}\text{P}_{0.5})_2$ is significantly more 3D than the $(\text{Ba,K})\text{Fe}_2\text{As}_2$ [28–30]. While it forms the outermost Γ -centered FS pocket in the $k_z = 0$ plane, the nearly non- k_z -dispersive d_{xy} pocket in $\text{BaFe}_2(\text{As}_{0.7}\text{P}_{0.3})_2$ has a size comparable to one of

the d_{xz}/d_{yz} FS (the odd combination of the d_{xz} and d_{yz} orbitals) at $k_z = \pi$ [17]. Consequently, one can expect enhanced scattering between the d_{xy} and d_{xz}/d_{yz} FSs, and thus possible charge transfer. The scenario of an anti-phase $d_{xy} - d_{xz}/d_{yz}$ charge transfer is illustrated in Figs. 4(c) and 4(d). In particular, on-site $d_{xy} \rightarrow d_{xz}/d_{yz}$ charge transfer occurring in opposite directions for neighbor Fe sites leads to the formation of two charge quadrupole moments with B_{1g} symmetry. Their nodes are along the $X'-Y'$ directions. In momentum space, these fluctuating charge transfer can induce a dynamic FS distortions with nodes along Γ -M and Γ -M', as illustrated in Fig. 4(h). As mentioned above, the removal of the σ_v and σ_d symmetry operations due to the As/P disorder couples the B_{1g} and B_{2g} symmetries, providing an explanation for the same oscillation frequencies in the B_{1g} and B_{2g} channels.

For completeness, we show in Figs. 4(e) and 4(f) that in-phase charge transfer between the d_{xy} orbital and the d_{xz}/d_{yz} orbitals is also possible. The fluctuating in-phase charge transfer induces the dynamic symmetric FS distortions illustrated in Fig. 4(i). The broad A_{1g} peak at 350 cm^{-1} can be interpreted as a collective excitation associated to a A_{1g} type of dynamic FS deformation.

In summary, we used Raman scattering to investigate the SC gap and collective excitations in SC $\text{BaFe}_2(\text{As}_{0.5}\text{P}_{0.5})_2$ ($T_c \approx 16 \text{ K}$). We observe a SC pair breaking peak at 54 cm^{-1} (6.7 meV) that appears below T_c in the A_{1g} channel. The linear decrease of the spectral weight suggests nodes in the SC gap structure. We identify spectral features associated with Pomeranchuk oscillations in the A_{1g} , B_{1g} and B_{2g} symmetry channels. Unexpectedly, these features are well-defined, which we attribute to the fact that these frequencies are larger than the Fermi energy of this system, thus preventing overdamping by electron-hole continuum. The degeneracy of the Pomeranchuk mode in the B_{1g} and B_{2g} symmetry channels is explained by the mixing of these two symmetry channels due to the removal of the σ_v and σ_d operations caused by As/P disorder. This disorder manifests itself by the absence of the pnictogen A_{1g} phonon normally detected in other Fe-based superconductors. Interestingly, the temperature regime at which the Pomeranchuk oscillations get underdamped coincides with a crossover regime from NFL to FL determined from transport. Our results indicate that the Pomeranchuk instability plays a critical role in the low-energy physics of this Fe-based superconductor.

This work was supported by grants from MOST (2015CB921301) and NSFC (11274362) of China. S.-F.W., H.-H.K., A.L., and G.B. acknowledge support from the NSF Grant No. DMR-1104884 for spectroscopic characterization of pnictide materials. H.-H.K. and G.B. acknowledge support from the US Department of Energy, Basic Energy Sciences, and Division of Materials Sciences and Engineering under Grant No. DE-SC0005463 for the data analyses.

-
- [1] Y. Nakai, T. Iye, S. Kitagawa, K. Ishida, H. Ikeda, S. Kasahara, H. Shishido, T. Shibauchi, Y. Matsuda, and T. Terashima, *Phys. Rev. Lett.* **105**, 107003 (2010).
- [2] K. Hashimoto, K. Cho, T. Shibauchi, S. Kasahara, Y. Mizukami, R. Katsumata, Y. Tsuruhara, T. Terashima, H. Ikeda, M. A. Tanatar, H. Kitano, N. Salovich, R. W. Giannetta, P. Walmsley, A. Carrington, R. Prozorov and Y. Matsuda, *Science* **336**, 1554 (2012).
- [3] P. Walmsley, C. Putzke, L. Malone, I. Guillaumon, D. Vignolles, C. Proust, S. Badoux, A. I. Coldea, M. D. Watson, S. Kasahara, Y. Mizukami, T. Shibauchi, Y. Matsuda and A. Carrington, *Phys. Rev. Lett.* **110**, 257002 (2013).
- [4] J. G. Analytis, H. Kuo, R. D. McDonald, M. Wartenbe, N. Hussey, and I. Fisher, *Nature Phys.* **10** (2014).
- [5] R. Fernandes, A. Chubukov, and J. Schmalian, *Nature Phys.* **10**, 97 (2014).
- [6] V. K. Thorsmølle, M. Khodas, Z. P. Yin, C. Zhang, S. V. Carr, P. Dai, and G. Blumberg, *Phys. Rev. B* **93**, 054515 (2016).
- [7] Y. Gallais, R. M. Fernandes, I. Paul, L. Chauvière, Y.-X. Yang, M.-A. Méasson, M. Cazayous, A. Sacuto, D. Colson, and A. Forget, *Phys. Rev. Lett.* **111**, 267001 (2013).
- [8] F. Kretzschmar, T. Böhm, U. Karahasanović, B. Muschler, A. Baum, D. Jost, J. Schmalian, S. Caprara, M. Grilli, C. Di Castro, J. G. Analytis, J.-H. Chu, I. R. Fisher and R. Hackl, *Nature Phys.* **12**, 560 (2016).
- [9] W.-L. Zhang, P. Richard, H. Ding, A. S. Sefat, J. Gillett, S. E. Sebastian, M. Khodas, and G. Blumberg, *arXiv:1410.6452* (2014).
- [10] P. Massat, D. Farina, I. Paul, S. Karlsson, P. Strobel, P. Toulemonde, M.-A. Méasson, M. Cazayous, A. Sacuto, S. Kasahara, T. Shibauchi, Y. Matsuda and Y. Gallais, *arXiv:1603.01492* (2016).
- [11] I. Y. Pomeranchuk, *Sov. Phys. JETP* **8**, 361 (1958).
- [12] V. Oganessian, S. A. Kivelson, and E. Fradkin, *Phys. Rev. B* **64**, 195109 (2001).
- [13] M. Nakajima, S. ichi Uchida, K. Kihou, C.-H. Lee, A. Iyo, and H. Eisaki, *J. Phys. Soc. Jpn.* **81**, 104710 (2012).
- [14] T. Yoshida, I. Nishi, S. Ideta, A. Fujimori, M. Kubota, K. Ono, S. Kasahara, T. Shibauchi, T. Terashima, Y. Matsuda, H. Ikeda, and R. Arita, *Phys. Rev. Lett.* **106**, 117001 (2011).
- [15] H. Suzuki, T. Kobayashi, S. Miyasaka, T. Yoshida, K. Okazaki, L. C. C. Amolode, S. Ideta, M. Yi, M. Hashimoto, D. H. Lu, Z.-X. Shen, K. Ono, H. Kumigashira, S. Tajima, and A. Fujimori, *Phys. Rev. B* **89**, 184513 (2014).
- [16] D. Hu, X. Lu, W. Zhang, H. Luo, S. Li, P. Wang, G. Chen, F. Han, S. R. Banjara, A. Sapkota, A. Kreyssig, A. I. Goldman, Z. Yamani, C. Niedermayer, M. Skoulatos, R. Georgii, T. Keller, P. Wang, W. Yu, and P. Dai, *Phys. Rev. Lett.* **114**, 157002 (2015).
- [17] Y. Zhang, Z.-R. Ye, Q.-Q. Ge, F. Chen, J. Jiang, M. Xu, B.-P. Xie, and D.-L. Feng, *Nature Phys.* **8**, 371 (2012).
- [18] T. Shimojima, F. Sakaguchi, K. Ishizaka, Y. Ishida, T. Kiss, M. Okawa, T. Togashi, C.-T. Chen, S. Watanabe, M. Arita, K. Shimada, H. Namatame, M. Taniguchi, K. Ohgushi, S. Kasahara, T. Terashima, T. Shibauchi, Y. Matsuda, A. Chainani, and S. Shin, *Science* **332**, 564 (2011).
- [19] T. Yoshida, S.-I. Ideta, T. Shimojima, W. Malaeb, K. Shinada, H. Suzuki, I. Nishi, A. Fujimori, K. Ishizaka, S. Shin, Y. Nakashima, H. Anzai, A. a. H. a. M. Arita, M. andIno, H. Kumigashira, S. Ono, K. andKasahara, T. Shibauchi, T. Terashima, Y. Matsuda, M. Nakajima, S. Uchida, Y. Tomioka, T. Ito, K. Kihou, C. H. Lee, A. Iyo, H. Eisaki, H. Ikeda, R. Arita, T. Saito, S. Onari, and H. Kontani, *Sci. Rep.* **4**, 7292 (2014).
- [20] M. Yamashita, Y. Senshu, T. Shibauchi, S. Kasahara, K. Hashimoto, D. Watanabe, H. Ikeda, T. Terashima, I. Vekhter, A. B. Vorontsov and Y. Matsuda, *Phys. Rev. B* **84**, 060507(R) (2011).
- [21] X. Qiu, S. Y. Zhou, H. Zhang, B. Y. Pan, X. C. Hong, Y. F. Dai, Man Jin Eom, Jun Sung Kim, Z. R. Ye, Y. Zhang, D. L. Feng and S. Y. Li, *Phys. Rev. X* **2**, 011010 (2012).
- [22] M. Rahnbeck, G. L. Sun, D. L. Sun, C. T. Lin, B. Keimer, and C. Ulrich, *Phys. Rev. B* **80**, 064509 (2009).
- [23] L. Chauvière, Y. Gallais, M. Cazayous, A. Sacuto, M. A. Méasson, D. Colson, and A. Forget, *Phys. Rev. B* **80**, 094504 (2009).
- [24] Y. J. Um, J. T. Park, B. H. Min, Y. J. Song, Y. S. Kwon, B. Keimer and M. Le Tacon, *Phys. Rev. B* **85**, 012501 (2012).
- [25] Z.-H. Liu, P. Richard, K. Nakayama, G.-F. Chen, S. Dong, J.-B. He, D.-M. Wang, T.-L. Xia, K. Umezawa, T. Kawahara, S. Souma, T. Sato, T. Takahashi, T. Qian, Yaobo Huang, Nan Xu, Yingbo Shi, H. Ding and S.-C. Wang, *Phys. Rev. B* **84**, 064519 (2011).
- [26] S. Thirupathaiah, D. V. Evtushinsky, J. Maletz, V. B. Zabolotnyy, A. A. Kordyuk, T. K. Kim, S. Wurmehl, M. Roslova, I. Morozov, B. Büchner, and S. V. Borisenko, *Phys. Rev. B* **86**, 214508 (2012).
- [27] Q. Q. Ge, Z. R. Ye, M. Xu, Y. Zhang, J. Jiang, B. P. Xie, Y. Song, C. L. Zhang, Pengcheng Dai and D. L. Feng, *Phys. Rev. X* **3**, 011020 (2013).
- [28] Z. R. Ye, Y. Zhang, F. Chen, M. Xu, Q. Q. Ge, J. Jiang, B. P. Xie, and D. L. Feng, *Phys. Rev. B* **86**, 035136 (2012).
- [29] J. G. Analytis, J.-H. Chu, R. D. McDonald, S. C. Riggs, and I. R. Fisher, *Phys. Rev. Lett.* **105**, 207004 (2010).
- [30] H. Shishido, A. F. Bangura, A. I. Coldea, S. Tonegawa, K. Hashimoto, S. Kasahara, P. M. C. Rourke, H. Ikeda, T. Terashima, R. Settai, Y. Ōnuki, D. Vignolles, C. Proust, B. Vignolle, A. McCollam, Y. Matsuda, T. Shibauchi, and A. Carrington, *Phys. Rev. Lett.* **104**, 057008 (2010).